Biochimica et Biophysica Acta 1858 (2016) 2070–2080

Contents lists available at ScienceDirect

Biochimica et Biophysica Acta

journal homepage: www.elsevier.com/locate/bbamem

Tethered bilayer membranes as a complementary tool for functional and structural studies: The pyolysin case

Giulio Preta [a], Marija Jankunec [a], Frank Heinrich [b], Sholeem Griffin [c], Iain Martin Sheldon [c], Gintaras Valincius [a,*]

[a] Department of Bioelectrochemistry and Biospectroscopy, Institute of Biochemistry, Vilnius University, Vilnius, Lithuania
[b] NIST Center for Neutron Research, Gaithersburg, MD 20899, USA
[c] Institute of Life Science, Swansea University Medical School, Swansea SA2 8PP, United Kingdom

ARTICLE INFO

Article history:
Received 24 February 2016
Received in revised form 27 April 2016
Accepted 17 May 2016
Available online 19 May 2016

Keywords:
Cholesterol-dependent cytolysins
Tethered bilayer membranes
Dynasore
Electrochemical impedance spectroscopy

ABSTRACT

We demonstrate the use of tethered bilayer lipid membranes (tBLMs) as an experimental platform for functional and structural studies of membrane associated proteins by electrochemical techniques. The reconstitution of the cholesterol-dependent cytolysin (CDC) pyolysin (PLO) from *Trueperella pyogenes* into tBLMs was followed in real-time by electrochemical impedance spectroscopy (EIS). Changes of the EIS parameters of the tBLMs upon exposure to PLO solutions were consistent with the dielectric barrier damage occurring through the formation of water-filled pores in membranes. Parallel experiments involving a mutant version of PLO, which is able to bind to the membranes but does not form oligomer pores, strengthen the reliability of this methodology, since no change in the electrochemical impedance was observed. Complementary atomic force microscopy (AFM) and neutron reflectometry (NR) measurements revealed structural details of the membrane bound PLO, consistent with the structural transformations of the membrane bound toxins found for other cholesterol dependent cytolysins. In this work, using the tBLMs platform we also observed a protective effect of the dynamin inhibitor Dynasore against pyolysin as well as pneumolysin. An effect of Dynasore in tBLMs, which was earlier observed in experiments with live cells, confirms the biological relevance of the tBLMs models, as well as demonstrates the potential of the electrochemical impedance spectroscopy to quantify membrane damage by the pore forming toxins. In conclusion, tBLMs are a reliable and complementary method to explore the activity of CDCs in eukaryotic cells and to develop strategies to limit the toxic effects of CDCs.

1. Introduction

Cholesterol-dependent cytolysins (CDCs) are a large family of β-barrel pore-forming toxins that are produced by Gram-positive bacteria [1,2]. Pore formation is strictly dependent on the presence of membrane cholesterol, which functions as the receptor for most CDCs. The pore-forming mechanism of the CDCs is a multistep process that involves recognition and binding to the cholesterol-containing membrane by domain 4 of the toxin, oligomerization of the soluble monomers on the target cell membrane to form a large pre-pore complex, and penetration of the pre-pore into the membrane to become a transmembrane pore [3,4]. Among the less-characterized CDCs, pyolysin (PLO) is the most important actively secreted virulence factor of *Trueperella pyogenes*, which is an opportunistic pathogen associated with suppurative infections, such as mastitis, septic arthritis, liver abscessation, pneumonia and endometritis [5,6]. Pyolysin has a distinct advantage for in vitro studies because PLO as well as intermedilysin is spontaneously active in vitro, whereas most other CDCs require thiol activation.

The dynamin inhibitor Dynasore, reduces the sensitivity of endometrial stromal cells as well as HeLa cells against PLO [7]. This effect was dynamin-independent and related to the targeting of cellular cholesterol and the disruption of plasma membrane lipid rafts, similar to positive control methyl-β-cyclodextrin [7].

Usually, CDCs activity is determined by in vitro assays using red blood cells or specific cell lines [8], however recently an alternative bioanalytical technique based on the use of tethered bilayer lipid membranes (tBLMs) was proposed [9]. The formation of defects or water-filled pores in tBLMs can be easily sensed and followed, in real-time, by electrochemical impedance spectroscopy (EIS) and opens the possibility of tBLMs use in bioanalytical applications [10,11]. In particular tBLMs are already largely used for protein membrane interaction studies, for reconstitution of functional protein complexes into membranes and ion channel activity monitoring [12,13].

In the present study we investigate the reconstitution of PLO into tBLMs, showing that the recombinant but not the mutant form of PLO specifically inflicts dielectric damage to tBLMs. Auxiliary structural techniques as atomic force microscopy and neutron reflectometry attest for localization of the intact toxin pores and prepore entities in tBLMs, thus confirming applicability of tBLMs as a sensitive, and less time

* Corresponding author.
E-mail address: gintaras.valincius@bchi.vu.lt (G. Valincius).

http://dx.doi.org/10.1016/j.bbamem.2016.05.016
0005-2736/

consuming molecular tools for sensing activity of pore-forming toxins. Earlier reported protective effect of Dynasore against PLO [7] has been also confirmed by tBLMs methodology, thus, proposing tBLMs as an innovative tool not only for the detection of the activity but also for the development of strategies to limit the impact of CDCs.

2. Material and methods

2.1. Tethered bilayer membranes

Tethered phospholipid bilayer membranes (tBLMs) were prepared on gold-coated glass slides by the vesicle fusion method as previously described [14]. Briefly, freshly gold-coated glass slides were immersed in a solution of the tether WC14 (20-tetradecyloxy-3,6,9,12,15,18,22-heptaoxahexatricontane-1-thiol; synthesized in-house), and β-mercaptoethanol (ßME) (Sigma-Aldrich, St. Louis, MO) mixed at molar ratio 30:70 to form mixed self-assembled monolayers (SAMs). After incubation, the slides were washed and dried in a stream of nitrogen gas. The tBLMs were formed by incubating the SAM with a solution of cholesterol/DOPC (phospholipids,1,2-dioleoyl-*sn*-glycero-3-phosphocholine) at a molar ratio of 40:60, which approximately mimics biological membrane compositions. The tether-functionalized gold films were assembled into an electrochemical setup with 8 independent vials, each with an area of 0.32 cm^2. The bottom of each vial was a patch of the tether-functionalized gold layer and is exposed to the solutions. Purified Milli-Q Plius (Millipore, USA) water was used for all buffers. The membranes were equilibrated with the working phosphate buffer for at least 30 min and only those tBLMs samples exhibiting stable parameters were used to test activity of CDCs. In most cases, at least 6 vials out of 8 exhibited excellent stability of parameters. DOPC and cholesterol used for membrane assembly were purchased from Avanti Polar Lipids (Alabaster, AL).

2.2. Electrochemical impedance measurements

Electrochemical impedance was measured using a universal electrochemical workstation Zennium (Zahner, Kronach, Germany) in the frequency range between 0.1 Hz and 100 kHz, with 10 logarithmically distributed measurement points per decade. A saturated silver–silver chloride (Ag/AgCl/NaCl (aq. sat.) microelectrode (M-401F, Microelectrodes, Bedford, NH) was used as reference, which has the potential +196 mV vs. standard hydrogen electrode while the auxiliary electrode was a platinum wire (99.99% purity, Aldrich; diameter = 0.25 mm) coiled around the barrel of the reference electrode. Measurements were carried out with 10 mV alternating current at 0 V bias versus the reference electrode in aerated solutions. The admittance of the tBLMs was calculated from the electrochemical impedance spectra according to a simple relation $Y = Z^{-1}$. Average admittance values were obtained from at least 3 independent tBLM for each treatment.

2.3. Atomic force microscopy (AFM)

Solid substrates for atomic force microscopy measurements were prepared as fresh cleaved mica (grade 4, SPI Supplies, USA) surfaces covered with the annealed gold layer (typically thickness was 30 nm, the adhesion Ti layer was 1 nm). The self-assembled monolayers on the substrates were obtained from the solution of WC14/ßME (30:70) in ethanol. Incubation time was 16 h. After incubation, the samples were rinsed with ethanol and dried under nitrogen stream and stored dry until usage. Before measurements the substrates with SAM were incubated with DOPC(60%)/Chol(40%) MLVs (multi-lamellar vesicles) for 1.5 h, during which tBLMs formed. After tBLMs formation, samples were repeatedly rinsed with 0.1 mM NaCl, 0.01 mM NaH_2PO_4, pH 7.2 buffer. The buffer solution containing 50 nM pyolysin was injected into the imaging cell and tBLMs sample was exposed to the pore-forming protein for 40 min. Then, solution in the cell was replaced with protein-free buffer and imaging stated immediately.

2.4. AFM imaging and image processing

Imaging was carried out in a tapping mode on a Dimension Icon (Bruker, Santa Barbara, CA, USA) scanning probe microscope system. Imaging was performed at the room temperature (20 ± 0.5 °C) using triangular SNL-C probes (Bruker, Santa Barbara, CA, USA). Radius of tips used in the study was 2–12 nm, spring constant k = 0.12–0.48 N/m, resonance frequency = 40–75 kHz. Multiple images of different scanning areas and angles were taken for each sample. Typically, the scans were performed in 512 × 512 pixel mode. Scan rates from 0.2 to 0.5 Hz. Samples with assembled tBLMs were submerged in the liquid all the time during the AFM experiments. Images were analyzed by WSxM [15] software. Reconstituted protein complexes (arcs and pores) were manually traced using DNA Trace software [16].

2.5. Neutron reflectometry

NR measurements were performed at the NGD-MAGIK reflectometer at the NIST Center for Neutron Research (NCNR) [17]. Reflectivity curves were recorded for momentum transfer values $0 \le q_z \le 2.5\ nm^{-1}$. tBLMs were prepared on 3′ diameter Silicon wafers assembled in a NCNR reflectometry flow cell [18]. Subsequent sample conditions were measured using three isotopically different bulk solvents (contrasts), i.e., aqueous buffer prepared from D_2O, H_2O, and a 2:1 mixture by volume of D_2O and H_2O (CM4). Self-assembled monolayers (SAMs) were prepared by overnight incubation of the gold-coated slides in ethanolic solution of the lipid tether compound HC18 (Z20-(*Z*-octadec-9-enyloxy)-3,6,9,12,15,18,22-heptaoxatetracont-31-ene-1-thiol). For each measured contrast, adequate counting statistics were obtained after 6 h. The flow cell allows for in situ buffer exchange; therefore, subsequent measurements were performed on the same sample area. The entire flow cell was maintained at 20.5 ± 0.5 °C. NR data were first collected from an *as*-prepared tBLMs. Thereafter, protein was added to the tBLMs and NR data was collected either during protein incubation or after rinsing the bilayer with buffer.

The 1D-structural profile along the lipid bilayer normal was modeled using a hybrid of a stratified slab model for the solid substrate [19], a continuous distribution model for the tBLMs [20], and a monotonic Hermite spline for the model-free envelope of the protein [21]. Individual slabs in the slab model were implemented for the bulk silicon, the silicon oxide, the chromium, and the gold layer. Fit parameters are thickness and neutron scattering length density (nSLD) for each layer, except for the bulk silicon. One global roughness fit parameter applies to all substrate interfaces. Individual sub-molecular groups implemented in the continuous distribution model are: βME, tether PEG chains, tether glycerol groups, substrate-proximal and substrate-distal PC and PS headgroups, substrate-proximal and substrate-distal methylene and methyl chains of lipid and tether molecules. Fit parameters are the bilayer hydrocarbon thickness for each bilayer leaflet, bilayer completeness, tether surface density, tether thickness, and βME surface density. One roughness fit parameter was applied to all distributions.

The Hermite spline that describes the volume occupancy profile of the protein is defined by control points, which are on average 2 nm apart. The spatial extension of the protein along the bilayer normal determines the number of control points, which is found iteratively during model optimization. Fit parameters for each control point are the volume occupancy of the envelope and the deviation from a position defined by equidistant control points throughout the spline. A constant nSLD is applied to spline functions that describe the volume occupancy of either completely protiated or deuterated protein material.

Data modeling was performed with the garefl and Refl1D software packages [18], using a differential evolution Markov chain global optimizer. Reflectivity curves recorded from one sample under different conditions were fitted simultaneously to the same model, sharing fit parameters, for example, for the solid substrate. The recorded Monte Carlo Markov Chain was used to determine the fit parameter confidence

limits using a statistical analysis, yielding a bias-free and objective estimate of the uncertainties of the resulting nSLD profiles while avoiding over-parameterization [21].

2.6. Toxins

Wild-type recombinant PLO (rPLO) was purified as previously described [22]. The mutant PLO (dsPLO) was a kind gift from Professor M. Palmer (University of Waterloo, Waterloo, ON, Canada), while pneumolysin (PLY) was a kind gift of Dr. M. Plečkaitytė (Vilnius University, Vilnius, Lithuania) and was generated as previously described [23].

2.7. Pre-incubation of PLO with cholesterol

For pre-blocking experiments rPLO protein (58 μg/100 μL) was incubated with 1 or 10 μL cholesterol dissolved in ethanol (0.386 mg/mL) for 30 min at room temperature prior to addition of the protein sample to the tethered membranes. As controls, ethanol alone, cholesterol dissolved in ethanol (final concentration 1 μM or 10 μM) and rPLO in ethanol (final concentration 10 nM) were also added to the membranes. All curves were recorded after 30 min.

2.8. Hemolysis assay

Hemolysis assay was performed as a functional measure of cytolytic activity, using a previously reported method [7,22,24]. To prepare the washed red blood cells, commercially available defibrinated horse blood (Oxoid, Basingstoke, UK) was centrifuged at 1500 ×*g* for 10 min, 4 °C. The supernatant was removed and the pelleted red blood cells were resuspended in PBS. The process was then repeated three to four times until the supernatant was colorless. Subsequently, 125 μL of the red blood cell pellet was added to 50 mL PBS to make a 0.25% final solution of washed red blood cells. The samples were incubated at 37 °C for 1 h with the toxins before centrifuging at 1500 ×*g* for 5 min at room temperature to pellet intact red blood cells. Finally, 200 μL of the resulting supernatant was transferred into a flat-bottomed 96-well plate (Fisher Scientific) before the OD_{405} of the supernatant was measured in a plate reader. The point at which 50% of the hemoglobin was released from the red blood cells was calculated

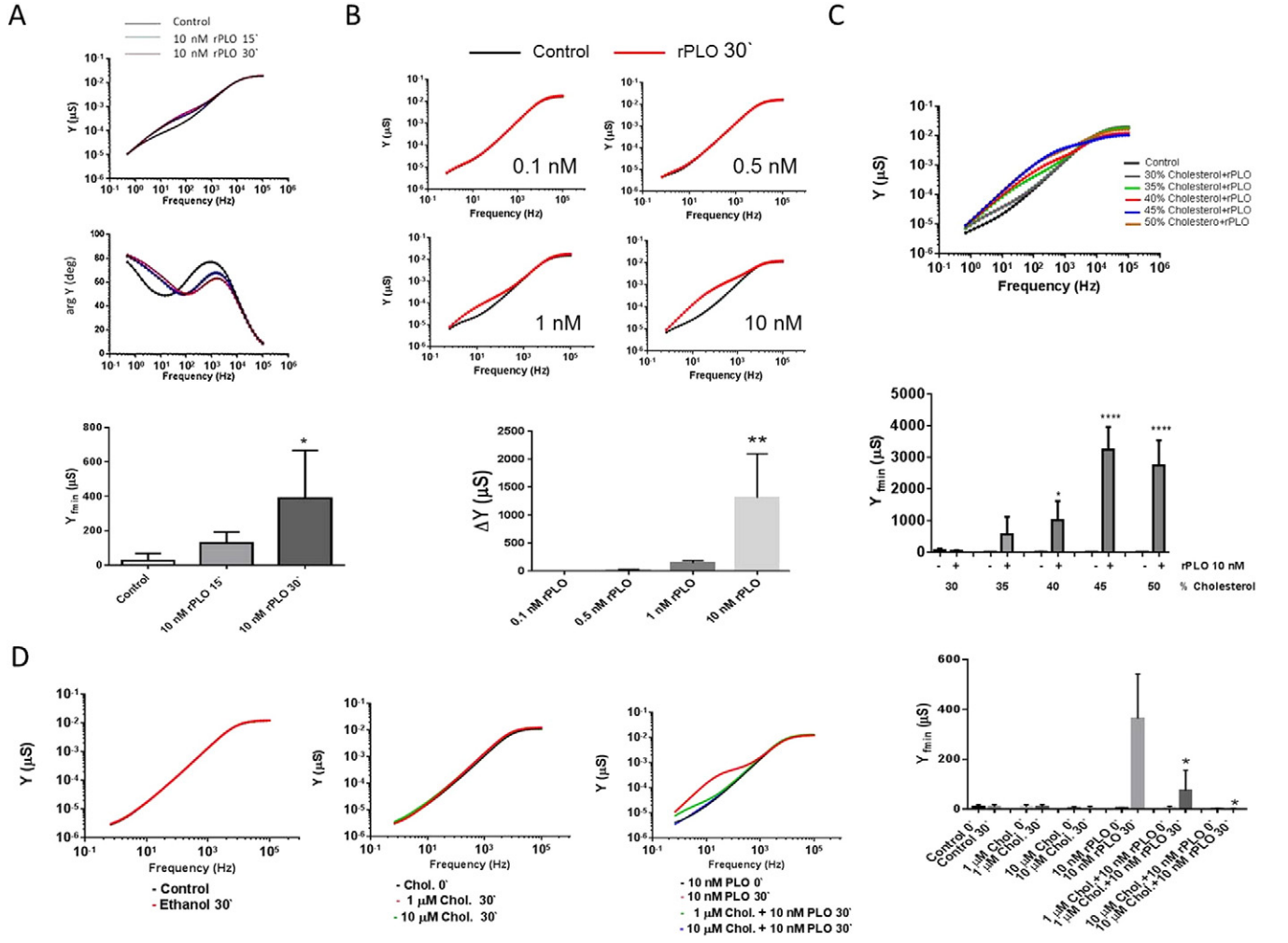

Fig. 1. rPLO induces dielectric damage to tBLMs in a time and dose-dependent way. A) tBLMs, formed by incubating the SAM with a solution of cholesterol/DOPC at a molar ratio of 40/60, were treated with 10 nM of rPLO and the admittance magnitude and phase were recorded after 15 and 30 min. The statistical analysis of the experiments is based on four independent experiments (One way ANOVA Dunnett's test). B) tBLMs, formed by incubating the SAM with a solution of cholesterol/DOPC at a molar ratio of 40/60, were treated with different concentration of rPLO and the admittance magnitude was recorded after 30 min. Statistical analysis of the experiments is based on three independent experiments and indicates the fold increase in admittance compared to control (One way ANOVA Dunnett's test). C) tBLMs, formed by incubating the SAM with a solution of cholesterol/DOPC with different concentrations of cholesterol (30%, 35%, 40%, 45% and 50%) were treated with PBS alone or PBS + 10 nM of rPLO and the admittance magnitude were recorded after 30 min. Statistical analysis is based on three independent experiments (One way ANOVA Bonferroni test comparing rPLO vs PBS). D) tBLMs formed by incubating the SAM with a solution of cholesterol/DOPC at a molar ratio of 40/60, were treated with ethanol as control, 1 or 10 μM cholesterol, 10 nM rPLO or 10 nM PLO pre-mixed at room temperature with 1 or 10 μM cholesterol for 30 min. The admittance magnitude was recorded after 30 min and statistical analysis of the experiments is based on three independent experiments (One way ANOVA Dunnett's test comparing rPLO vs rPLO pre-mixed with cholesterol).

graphically using the solver function of Microsoft Excel (Microsoft Corporation), setting the positive and negative controls as the maximum and minimum limits, respectively.

2.9. Confocal microscopy

Fluorescence microscopy imaging of tBLMs was performed on Zeiss LSM 700 inverted confocal microscope (Carl Zeiss, Oberkochen, Germany) using fluorescently labeled cholesterol derivatives described earlier [25]. Gold coated slides were placed on the bottom of small Petri glass and the tBLMs were exposed to a Helium neon laser 633 nm. In Dynasore experiments, tBLMs were treated with different concentrations of Dynasore for 30 min before acquisition of the data. Washout experiments were performed rinsing 3 times the Dynasore solution, with PBS pH 7.4, before acquiring new images. Intensity of the staining was calculated using the ImageJ software (National Institutes of Health, Bethesda, MD, USA). Statistical analysis is based on the quantification of MOD (Mean Optical Density) of 40 different regions from two separate experiments.

2.10. Statistical analysis

tBLMs data and hemolysis data are presented as the arithmetic mean (SD) of at least 3 independent experiments. Statistical analyses were performed using GraphPad Prism, version 6 (La Jolla, CA, USA), and data were analyzed using one way ANOVA Dunnett's test except where stated differently. Significance was ascribed at $P < 0.05$.

3. Results

3.1. Electrochemical impedance of tBLMs is affected by rPLO

Injection of rPLO into the buffer solution in contact with tBLMs triggers changes in the electrochemical impedance (EI) spectra of those tBLMs that contain cholesterol. With no rPLO added, the Bode graphs (admittance representation) of EI exhibit typical tBLMs shapes (Fig. 1A). The admittance magnitude, Y, plot exhibits sigmoidal shape, with the upper step determined by a solution resistance, and the bottom step-like feature determined by a residual defect density in tBLMs [10]. The phase of admittance, arg Y, exhibits a minimum corresponding to a low frequency step, while, in the high frequency range one may observed a downward trending curve. The addition of rPLO triggers changes in the low-frequency part of the spectra. The high frequency part remains unaffected (Fig. 1A). The extent of membrane damage can be conveniently assessed by two characteristic points on the Bode plots: 1) frequency f_{min} [10,26], at which low frequency range admittance minimum occurs, and 2) the admittance magnitude value at this frequency point $Y_{fmin} = Z_{fmin}^{-1}$ [10,12,26,27]. As recently shown [26], both f_{min} and Y_{min} are dependent from the density of defects in tBLMs. However, within existing theoretical framework [10], for exact numerical evaluation of a number of membrane damaging PLO entities in tBLMs one needs to assume homogeneous distribution and monodispersity of the physical properties of the defects. In this work, we will restrict our analysis to a qualitative comparison and use Y_{min} values to compare EIS changes induced by rPLO under different conditions.

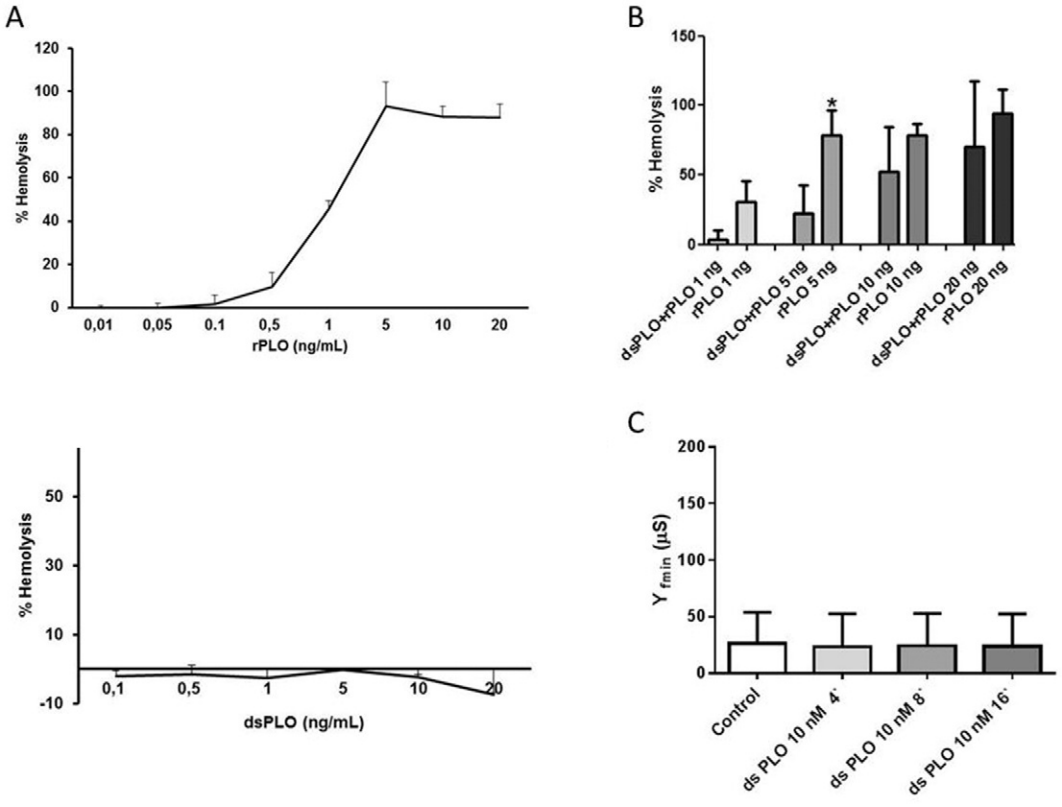

Fig. 2. The mutant version of PLO (dsPLO), does not possess hemolytic activity and does not inflict dielectric damage to tBLMs. A) Washed red blood cells were treated with different doses of rPLO or dsPLO and the hemoglobin released was evaluated by reading the OD_{405} of the supernatant in a plate reader. Data are shown as % of the hemolysis compared to 100% hemolysis induced by incubating red blood cells with a 0.1% solution of Triton X-100. B) Washed red blood cells were treated with different doses of rPLO alone or a mix of rPLO and dsPLO at a ratio of 1:1 and the hemoglobin released was evaluated by reading the OD_{405} of the supernatant in a plate reader. Data are shown as % of the hemolysis compared to 100% hemolysis induced by incubating red blood cells with a 0.1% solution of Triton X-100 (positive control). Statistical analysis of the experiments is based on three independent experiments and indicates the % of hemolysis compared to positive control (One way ANOVA Bonferroni test comparing rPLO vs dsPLO/rPLO). C) tBLMs, formed by incubating the SAM with a solution of cholesterol/DOPC at a molar ratio of 40/60, were treated with 10 nM of dsPLO at different time points. Statistical analysis presented is based on three independent experiments and indicates the admittance values expressed in microSiemens (One way ANOVA Dunnett's test).

As seen in Fig. 1, rPLO-induced EI spectral changes were found to be time dependent (Fig. 1A with statistical analysis below) and concentration dependent (Fig. 1B with statistical analysis below) with detectable changes in admittance starting from 1 nM rPLO. Similar EIS response was observed for other pore-forming toxins such as αHL [28,29] and vaginolysin [9]. To elucidate the concentration dependent nature of the rPLO–membrane interaction, all curves in Fig. 1B were recorded 30 min after injection. Concentration dependence of admittance vs. rPLO concentration is nonlinear and the toxin effect starts manifesting in EIS curves at around 1 nM concentration of protein. Because rPLO belongs to a class of CDC, one may expect that the concentration of cholesterol in phospholipid bilayer will affect the damage inflicted by rPLO to the membrane integrity. Such an effect is clearly demonstrated by the data in Fig. 1C (statistical analysis below). At a toxin concentrations of 10 nM the rPLO-induced Y_{fmin}, depends non-linearly on the cholesterol concentration in the tBLMs. At low cholesterol content (30%), only a marginal increase of the tBLMs admittance is detected. More remarkable increase develops at higher cholesterol concentrations (>30%) clearly indicating that cholesterol is an essential component for activating the ability of rPLO to inflict damage to tBLMs. Such a concentration-dependent effect of cholesterol on tBLMs was already reported for other CDCs [9]. Interestingly, above 45% of cholesterol a slight decrease of the membrane damage, as recorded by the EIS, was observed. To further confirm the cholesterol-dependent nature of the membrane inserting PLO, we performed pre-blocking studies with cholesterol, already performed in literature [30]. As seen in Fig. 1D, pre-incubation of rPLO protein with cholesterol prior to its addition to membranes, resulted in dose-dependent abrogation of rPLO-induced dielectric damage to tBLMs. An ethanol carrier control was also included which showed no effect on membrane conductance. These results further demonstrate the cholesterol-dependent nature of PLO for membrane insertion and pore formation.

3.2. Mutant rPLO without hemolytic activity

A pyolysin mutant (dsPLO) with an engineered disulfide bond between domains 2 and 3 which binds to membranes but does not form oligomers was previously described [31]. This mutant showed no hemolytic activity on horse red blood cells compared to the rPLO (Fig. 2A). Moreover, pre-incubation of red blood cells with the mutant form dsPLO reduced the hemolytic activity of rPLO when the two toxins are used at ratio 1:1 demonstrating that the two forms compete for binding to membrane cholesterol (Fig. 2B). Injection of dsPLO into the buffer does not trigger admittance changes of tBLMs (Fig. 2C) confirming that the EIS recorded effects are related to the induced phospholipid bilayer damage by rPLO. The morphology of these species was visualized by the atomic force microscopy.

3.3. Visualization of PLO oligomers in tBLMs

As seen in Fig. 3 several typical shapes of rPLO species in tBLMs were observed by the AFM. Upon reconstitution into tBLMs, pyolysin mainly forms incomplete pores, which are seen as protruding above the surface of tBLMs arc-shaped structures. The protrusion of the protein oligomers into the aqueous bulk, as measured by the profile of the cross section (Fig. 3D), typically amounts to 6 nm. To collect statistical information

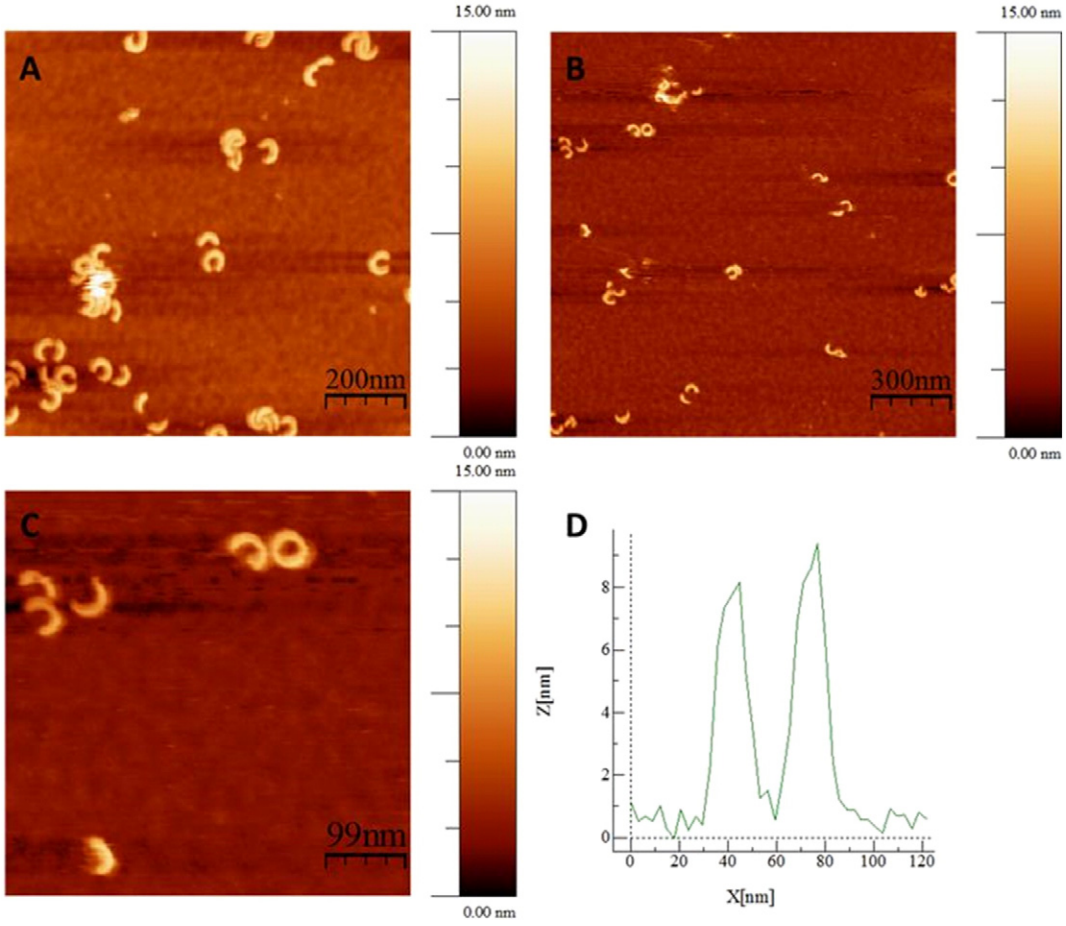

Fig. 3. Visualization of PLO oligomers in tBLMs by AFM. AFM topography images of tBLMs (cholesterol/DOPC 40/60) after incubation with 50 nM of pore forming toxin – pyolysin for 40 min: A) image scan size 1 μm × 1 μm, B) image scan size 1.5 μm × 1.5 μm, C) and D) enlarged view (from panel B) of pore and its profile (500 nm × 500 nm). Table 1 reports the dimensional parameters of PLO oligomers in the artificial membrane.

Table 1
Lateral and normal dimensions of rPLO oligomer entities visualized in Fig. 3.

Entity	Average height, nm	Average length, nm
≤1/2 ring	6.18 ± 0.60	58.33 ± 9.27
≈1/2 ring	5.90 ± 0.49	73.13 ± 16.12
≥3/4 ring	5.95 ± 0.64	113.00 ± 0.00

about the sizes of the entities visible in Fig. 3 we performed the statistical analysis of the arcs by the DNA Trace software. The individual PLO arcs were manually traced with a step size of 2 nm. The inner and outer PLO diameters of complete pores measured as FWHM (Fig. 3D) were $d_{inner} = 18.29 \pm 1.03$ nm and $d_{outer} = 46.51 \pm 3.47$ nm, respectively. Incomplete pores, as measured for 1/2 circle entities, were slightly bigger. Their radius was $r_{outer} = d_{outer}/2 = 28.7 \pm 6.28$ nm. These values are in line with scanning electron microscopy of red blood cells subjected to PLO [32] or with the pore sizes measured for other members of the cholesterol-dependent cytolysins family [33].

Table 1 summarizes heights of the objects above the surface of tBLMs. Slight difference can be discerned between different oligomers in tBLMs. However, given the intervals of errors in Table 1, one may claim only marginal differences in the size along the normal to a tBLM surface. On average, both complete and incomplete ring entities are protruding above the phospholipid membrane by about 6 nm.

3.4. Insertion of PLO into phospholipid bilayer probed by neutron reflectometry

While AFM provides structural data (with different resolution) both laterally and along the normal to a surface, this technique is incapable of visualizing protein material distribution inside the bilayer. Neutron reflectometry provides an experimental alternative to visualize pore-forming protein insertion into the membrane. Neutron reflectivity data in Fig. 4 present the profiles of distributions of different components of tBLMs during/after the incubation of tBLMs with mutated dsPLO form (Fig. 4A), rPLO at pH 7.0 (Fig. 4B) and pH 4.5 (Fig. 4C). Red bold line depicts the distribution of the protein inside and outside the membrane. Meaning of other color lines explained in the legend in Fig. 4.

In case of the mutated form of PLO, the protein volume fraction trace is mainly located outside of the tBLMs (at $z > 7.5$ nm, where z is an arbitrary plane at the surface of the gold layer). The protein profile extends approximately by 10–12 nm into the solution. However, some non-zero trace is also observed between z from 4 nm to 7.5 nm, an interval mainly coinciding with the position of the distal to a solid surface leaflet of the tBLMs. Fig. 4B that displays protein (and other components) distribution after the exposure to rPLO solution (at 190 nM concentration), clearly indicates a redistribution of the protein trace. Here the fraction of the protein outside of the tBLMs is decreased, while more of the protein is located within the hydrophobic core of the tBLMs. Quite

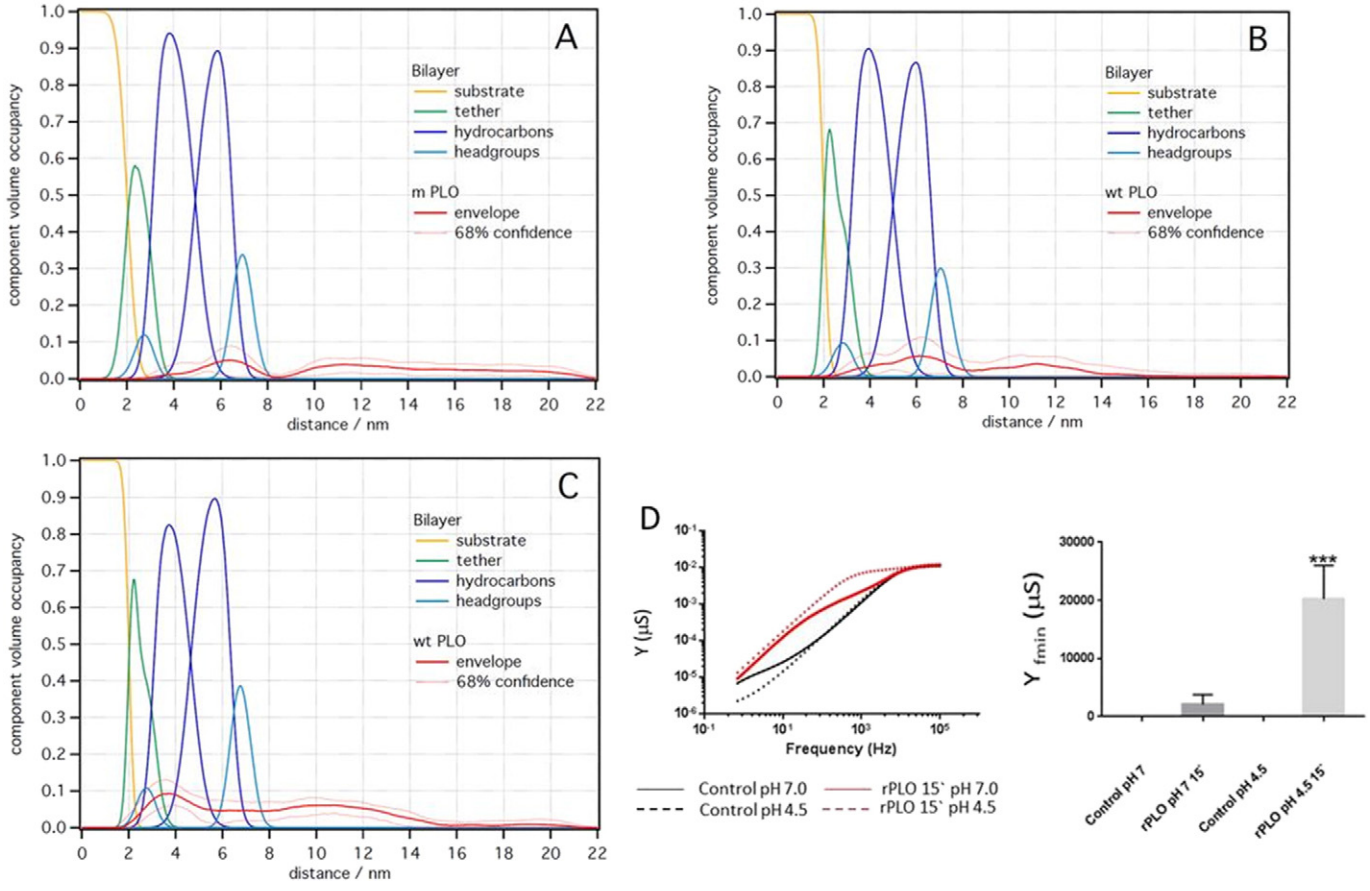

Fig. 4. Insertion of PLO into phospholipid bilayer probed by neutron reflectometry: tBLM component volume occupancies. A) Cholesterol/DOPC tBLM at molar ratio 40/60 after exposure to 87 nM of a mutated dsPLO for the whole time of reflectivity curve acquisition (approximately 6 h); B) same neat tBLM after the exposure to 180 nM of a wild type rPLO for 60 min at pH 7.0, and then rinsing the system with protein-free buffer; C) same neat tBLM after the exposure to 180 nM of a wild type rPLO for 60 min at pH 4.5, and then rinsing the system with protein-free buffer; D) tBLMs, formed by incubating the SAM with a solution of cholesterol/DOPC at a molar ratio of 40/60, were treated with 10 nM of rPLO in buffer at pH 7 or 4.5 and the admittance magnitude was recorded after 15 min. The curve fit allowed protein spline to be fitted to elucidate systematic uncertainty. Statistical analysis presented is based on three independent experiments and indicates the admittance values expressed in microSiemens (One way ANOVA Dunnett's test).

Table 2
Distribution of PLO volume fractions in the tBLMs.

Region of tBLMs	Protein volume fractions		
	dsPLO present in the solution at pH 7.0	rPLO (incubated at pH 7.0)	rPLO (incubated at pH 4.5)
Proximal leaflet/headgroups	0.00 ± 0.01	0.02 ± 0.05	0.06 ± 0.04
Proximal leaflet/hydrophobic slab	0.05 ± 0.07	0.12 ± 0.10	0.18 ± 0.09
Distal leaflet/hydrophobic slab	0.13 ± 0.10	0.20 ± 0.13	0.12 ± 0.07
Distal leaflet/headgroups	0.08 ± 0.07	0.10 ± 0.07	0.06 ± 0.03
Aqueous bulk	0.71 ± 0.14	0.50 ± 0.19	0.55 ± 0.10

surprisingly, we discovered some change in protein material distribution within the membrane when protein reconstitution pH is lowered to pH 4.5. As seen in Fig. 4C, at pH 4.5 penetration of the protein into the proximal compared to the distal leaflet increases. The protrusion of the protein complex into the aqueous phase, in this case, remains about the same as at pH 7.0 and amounts to approximately 7 nm (the protein trace at $z > 15$ nm, is obviously below the error level). The estimates of the protein volume fraction are summarized in Table 2.

Fig. 4B and C also allows comparing relative volume fractions of the phospholipid head groups following the rearrangement of protein within the bilayer. In particular, at pH 7.0 (Fig. 4B) the ratio of the volume densities of the head groups in proximal and distal leaflets is

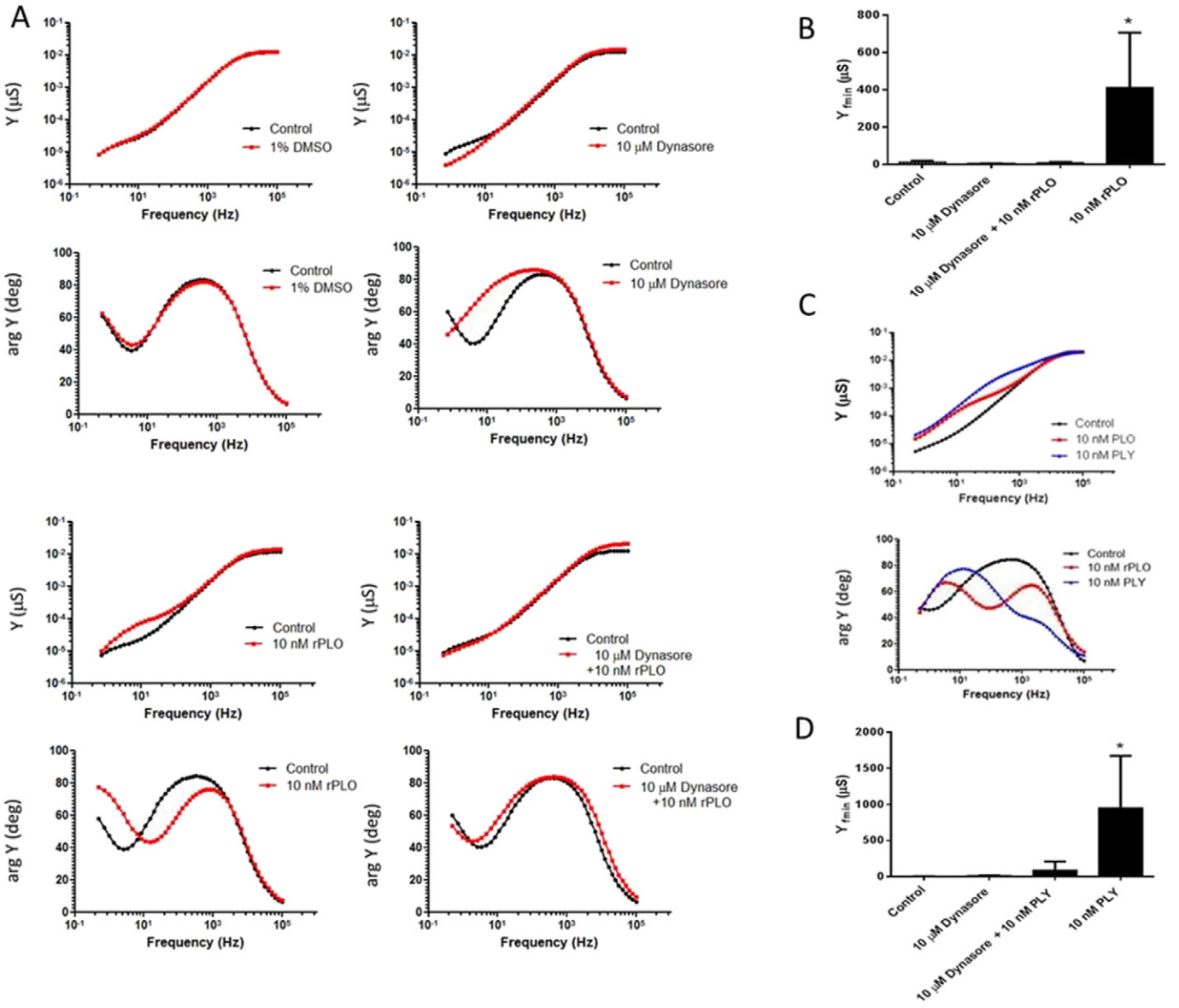

Fig. 5. Dynasore protects against the dielectric damage induced by PLO and PLY. tBLMs, formed by incubating the SAM with a solution of cholesterol/DOPC at a molar ratio of 40/60, were treated for 30 min with 1% DMSO alone, 10 μM Dynasore, 10 nM rPLO or by 10 μM Dynasore followed after incubation for 30 min by 10 nM rPLO. The admittance magnitude (Mod Y) and phase (Arg Y) were recorded after 30 min. B) Statistical analysis of Fig. 5A based on three independent experiments (One way ANOVA Dunnett's test). C) Statistical analysis of three independent experiments performed like in Fig. 5A but using 10 nM of PLY instead of PLO (One way ANOVA Dunnett's test).

approximately 13/17, while pH decrease to 4.5 results in change of the ratio to 3/16 consistent with the protein volume fraction increase in the proximal leaflet (Fig. 4C). In other words, at pH 7.0 larger portion of protein is predominantly located in the distal leaflet of the tBLMs. According to Table 2 data, lowering the pH facilitates full insertion of the protein into the bilayer, thus, one would expect more structural and, presumably, functional damage to an insulation properties of the bilayer membrane. The EIS data recorded at pH 4.5 and pH 7.0 clearly indicates correlation with neutron reflectometry: lowering the pH drastically amplified protein-induced EIS spectral changes (Fig. 4D). The rPLO induced change of Y_{min} (Fig. 4D), a parameter that is proportional to a density of defects in the membrane [10,26], was considerably bigger at pH 4.5 compared to the change at pH 7.0.

3.5. Protective effect of Dynasore against the dielectric damage induced by CDCs

It was previously reported that the dynamin inhibitor Dynasore protected stromal cells against PLO and SLO induced cytolysis. This effect was dynamin independent and related to targeting of cellular cholesterol [7]. To better evaluate the effect of Dynasore on cholesterol we tested if Dynasore can influence the dielectric damage induced by rPLO on tBLMs. Pre-incubation of Dynasore (30 min), remarkably reduces the effect of the toxin (30 min/10 nM) on tBLMs (Fig. 5A). This effect was not due to the vehicle since incubation with 1% DMSO had no effect on tBLMs while incubation with Dynasore alone slightly influences the admittance of the membranes (Fig. 5 and quantification Fig. 5B). To exclude the possibility that the protection conferred by Dynasore was related to binding between Dynasore and rPLO, we performed an experiment where tBLMs were treated with a mix of Dynasore and rPLO: in this case, rPLO was still capable to induce a dielectric damage on tBLMs (Supplementary Fig. 1).

These data were further strengthened by the observation that Dynasore has protective effect against the dielectric damage induced by other CDCs like pneumolysin (PLY) (Fig. 5C), confirming that Dynasore has an effect on cholesterol within tBLMs, similar to the one previously observed in cells [7].

3.6. Dynasore decreases the staining of Cy5-cholesterol tBLMs

Fluorescent analogs of natural lipids and cholesterols have been designed and synthesized, allowing reaching the selective affinity to different regions of bilayers [34,35]. To evaluate the effect of Dynasore on Cy-5-cholesterol/DOPC derived tBLMs, we treated the membranes with different amount of Dynasore before confocal microscope analysis. As shown in Fig. 6A and quantified in Fig. 6B, Dynasore decreased the fluorescence, binding to cholesterol/DOPC, in a dose-dependent manner. However, the interaction seems to be rather weak, since the staining could be partially restored by washing Dynasore away from the solution (Fig. 6C and D). The role of Dynasore on cholesterol homeostasis in cells, however seems to be more complex and related to dynamin dependent and independent effects [7,36,37].

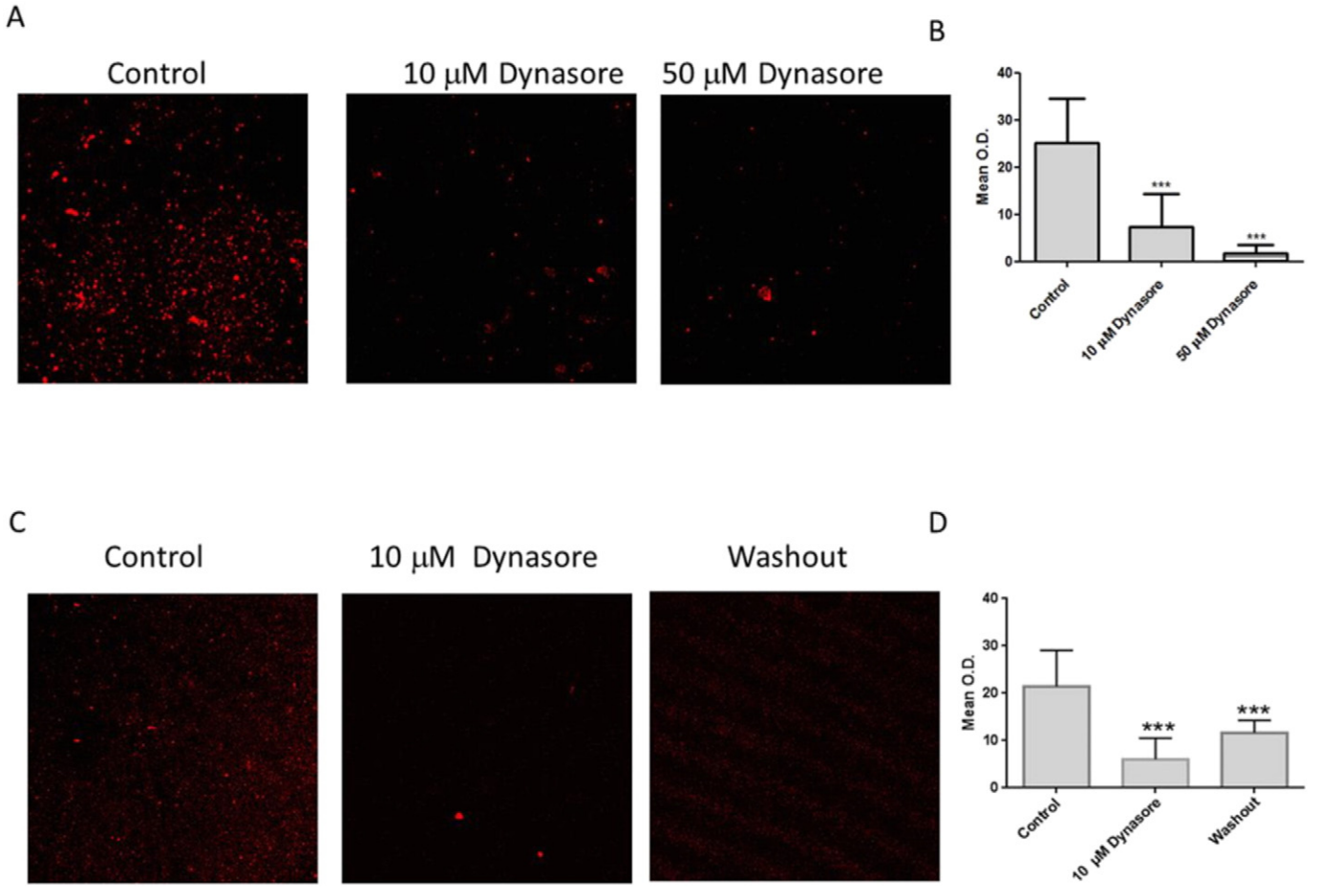

Fig. 6. Reversible decreasing of Cy5-cholesterol tBLMs staining by Dynasore. A) tBLMs, formed by incubating the SAM with a solution of cholesterol/DOPC at a molar ratio of 40/60 and containing 5% Cy5-cholesterol were analyzed by confocal microscopy with a Helium neon laser 633 nm. Dynasore was added at the reported concentration and incubated for 30 min before analysis. Statistical analysis is based on the quantification of MOD of 40 different regions from two separate experiments. (One way ANOVA Dunnett's test); B) tBLMs prepared like in A were analyzed by confocal microscopy with a Helium neon laser 633 nm. Dynasore was added at 10 μM concentration and incubated for 30 min before analysis. After acquisition of the images, Dynasore was washed out, rinsing tBLMs three times in PBS pH 7.4 before images were acquired again. Statistical analysis is based on the quantification of MOD of 40 different regions from two separate experiments (One way ANOVA Dunnett's test).

4. Discussion

Artificial membranes tethered to a surface are emerging as biologically relevant models for studying interactions between CDCs with phospholipid membranes. In this work we examined the reconstitution of PLO from *T. pyogenes* into tBLMs by electrochemical impedance spectroscopy. Our data show that rPLO impairs the dielectric/insulating function of the phospholipid membranes. Exposure of tBLMs to rPLO triggers EIS spectral changes in a way consistent with the formation of the dielectric, presumably, water-filled defects in bilayer. In particular, the step-like kink near 1 Hz on the log Y vs. log frequency curve shifts upwards, while the arg Y minimum point moves towards the higher frequencies. These changes are consistent with an increasing number of ion-conducting defects in tBLMs [10]. The density of the rPLO-induced defects increases in a time-dependent (Fig. 1A) and rPLO concentration dependent manner (Fig. 1B). These EIS changes are irreversible. This means that the initial state of tBLMs cannot be restored by removing toxin from the system. This type of damage is common for other pore-forming toxins, which attach to and oligomerize on the surface of the phospholipid bilayers [8,22]. Moreover, to confirm the cholesterol-dependent nature of pyolysin we performed experiments where PLO was pre-incubated with different amounts of cholesterol prior to its addition to tethered membranes. This approach had previously been used by others who had shown that pre-incubation with cholesterol blocked the dielectric damage inflicted to tethered membranes [30]. Our results clearly showed that cholesterol is acting as a potential binding or docking site for PLO, confirming the requirement of cholesterol for the activity of this toxin.

To exclude the possibility that the observed EIS results are not related to a non-specific protein adsorption to a membrane surface [38] or an insertion of protein that leads only to an increase in the dielectric constant [39], we used a mutant version of PLO (dsPLO), which is able to bind to cholesterol without forming pores [31]. In dsPLO the molecular fragment of the protein involved in oligomerization is chemically modified so, the pore-formation is inhibited. Injection of dsPLO does not trigger changes in the EI spectra of tBLMs as well as does not possess any hemolytic activity once tested on red blood cells (Fig. 2). At the same time, as it is obvious from the neutron reflectometry data (Fig. 4) a considerable amount of protein attaches to a surface and even penetrates into outer lipid leaflet of tBLMs (Table 2). However, in contrast to the rPLO, the larger portion (70%) of dsPLO is located outside the bilayer extending into solution up to 12 nm.

Such a large protrusion into the solution is resonating with the structural data obtained by the electron microscopy of the reconstituted pneumolysin [40]. In this work, the authors detected the pre-pore structural state of PLY oligomers which rise above the surface of the phospholipid by 10 nm, and penetrates outer leaflet by 2 nm. These structural parameters are very close to neutron reflectometry data obtained in the current work (Fig. 4, Table 2), however, we did not observe oligomer species rising >6–7 nm above the phospholipid bilayer. This fact suggests that protein bilayer complexes seen by the neutron reflectometry comprise a population of scattered across the surface cholesterol bound monomers of PLO. Individual protein monomer cholesterol complexes should exhibit sufficiently high surface mobility, so, these complexes should be invisible for relatively sluggish AFM scan modes available on our AFM equipment.

The comparison of AFM data (Table 1) and neutron reflectometry (Fig. 4) reveals interesting parallelism. Both incomplete arc-shaped pre-pores and complete ring-shaped pores of PLO are about the same height as measured by the AFM (Fig. 3 and data in Table 1). Neutron reflectometry data is consistent with AFM. It indicates that the main volume fraction of the protein material in aqueous phase extends by approximately 6–7 nm from the bilayer surface. As seen in Fig. 4B and C, some very low level protein volume fraction trace can be discerned up the distance of 10–12 nm, from the surface of the membrane, however, the level of the signal is completely overwhelmed by the standard error ribbon, so one cannot make unambiguous claims about the presence of the protein material beyond 6–7 nm from the surface. Taken together AFM and NR data does not indicate presence of the pre-pore state complexes of rPLO toxin similar to one observed in the case of PLY [40].

Neutron reflectometry allowed us to discover interesting structural transformation occurring mainly within the phospholipid sheet of the bilayer. If the pH of the rPLO reconstitution solution is lowered to 4.5, neutron reflectometry revealed quite significant rearrangement of the protein material distribution within the phospholipid bilayer (Fig. 4B and C). In particular, at pH 4.5 the membrane bound rPLO oligomers penetrate into the proximal leaflet of the tBLMs much deeper compared to protein reconstituted at pH 7.0. Electrochemical impedance follows these structural changes with significantly increased rPLO-induced change of Y_{min} (Fig. 4D), thus suggesting that the extent of the dielectric damage measured within fixed interval of time (30 min) is larger. Quite likely, lowering the pH facilitates penetration of oligomers into the bilayer, by accelerating rate determining steps of a multi-step process of reconstitution of cholesterol dependent rPLO. The acceleration of pore-forming protein reconstitution into both black lipid membranes and tBLMs was reported earlier for heptamer oligomers of α-hemolysin [28]. While α-hemolysin and rPLO reconstitution mechanism may be quite different (α-hemolysin, in contrast to PLO, is not strictly dependent on cholesterol), the observed parallelism between these two toxins hints at common steps in the process of reconstitution/oligomerization mechanism that are affected by pH variation in a similar fashion.

Quite surprisingly, the effect of pH on reconstituted rPLO is different. If the rPLO was first reconstituted at pH 7.0, rinsed with protein-free buffer and then the pH lowered to 4.5 a qualitatively different effect on Y_{min} was observed. In this case, lowering the pH resulted in Y_{min} to decrease (data not shown). The effect was much weaker than the one described above; the nature of it is not fully clear. It may not necessarily be related to the presence of PLO in the membrane because the same effect was observed when measuring Y_{min} response to pH variation on pristine tBLMs. Such tBLMs contain only naturally occurring defects, but no pore-forming toxins. The decrease of conductance (admittance in case of EIS) quitely contrasts the reaction to pH variation of the small diameter (1–2 nm) water-filled pores produced by α-hemolysin. Pores of α-hemolysin transitions from lower to higher conductance states as pH changes from 7.5 to 4.5 [41], which consequently leads to increased conductance. Taken together one may conclude that the pH variation strongly affects process of rPLO reconstitution, causing deeper penetration of rPLO oligomers into the bilayer at low pH. However, while reconstituted, the protein function and structure change little, pointing to an irreversible nature of the rPLO reconstitution. The molecular basis of pH dependence has been extensively investigated for Listeriolysin O (LLO) [42] but pH mediated activity was also reported for other members of the CDCs family [43]. Moreover, this result underlines the importance of tBLMs as a valid approach to study the modification of the activity of CDCs in function of external and internal factors including temperature, pH and ionic strength [44].

Biological relevance of the interaction between rPLO and the tBLMs could be verified by comparing the effects in tBLMs and hemolytic activity measured in cell culture. It is believed that pore formation in cell membrane is the primary reason for the cytotoxicity of PLO. Correlation of EIS features that are typical in the presence of water-filled defects with hemolytic activity would prove the existence of such pores and provide the biological basis for sensing and detection of this virulence factor by tBLMs-based sensors. The sensitivity of our tBLMs sensor, which is determined by the residual specific admittance of the membrane, is around 1 nM. This concentration is lower than that achieved by optical techniques utilizing tBLMs [45]. The requirement for cholesterol is proved from the fact that even at rPLO concentrations as high as 10 nM membrane damaging activity can be essentially nullified by decreasing the tBLMs cholesterol content below 30%. The limited data on the physiologic concentrations of pore-forming toxins currently

does not allow the conclusion that the sensitivity achieved in this work is sufficient to detect PLO in biological specimens however, in cultivation media of pathogenic bacteria, the levels of PLO could reach higher concentrations, being easily detectable.

By using tBLMs we were also able to confirm the reported protective effect of the dynamin inhibitor Dynasore against PLO as well as other CDCs [7]. Dynasore was discovered as a dynamin inhibitor and inhibits the clathrin-endocytic pathways, by blocking coated vesicle formation within seconds [46,47]. Dynasore was reported to control cholesterol trafficking and sterol-sensitive genes transcription in human HeLa cells and macrophages in a dynamin-dependent way [36]. However, more recent data suggested a dynamin-independent role of Dynasore on cholesterol homeostasis [7] in line with the observed off-target effects of this compound [37,48]. Using tBLMs we were able to confirm that Dynasore has an effect on cholesterol/DOPC membranes, which in this case is passive and related to surface binding. This is a general mechanism, valid also for other CDCs like PLY and is not dependent on an interaction of Dynasore with PLO since injection at the same time of PLO and Dynasore is capable to induce dielectric damage to tBLMs.

5. Conclusion

Our study highlighted the possible use of tBLMs for a fast, automated, real time detection of pyolysin as well as other CDCs in biological samples and in cultivation media. Through different approaches including EIS, AFM and neutron reflectometry, we have demonstrated the sensitivity and specificity of tBLMs towards the effect of pyolysin, a rather unique toxin in the family of CDCs since it does not require thiol activation to oligomerize. The reliability of our system was challenged by using mutant version of the toxin (dsPLO) which does not inflict dielectric damage to tBLMs, perfectly matching the absence of hemolytic activity observed in red blood cells [31]. Furthermore with tBLMs we were able to confirm the protective effect of Dynasore against PLO as well as PLY, already reported before in biological samples [7], opening the road to the excited possibility to use these artificial membranes for the development of strategies to limit the impact of CDCs. The relevance of the importance of further studies on tBLMs is underlined by the recently reported reconstitution of membrane proteins in artificial membrane systems [49] creating an ideal platform for exploring their potential for pharmacological or biotechnological uses. Different versions of lipids have been used as model building blocks to generate membranes homologue, as vesicular structures in solution (liposomes) [50], or as, tethered bilayer membrane, already tested against different toxins [9,29,51], in nanoparticle studies [52] and with soluble amyloid-beta oligomers [39]. Further improvements could still be reached related to the sensitivity of tBLMs with more detailed studies on the characteristics and properties of anchor molecules, a field continuously developing.

Supplementary data to this article can be found online at http://dx.doi.org/10.1016/j.bbamem.2016.05.016.

Competing interests

The authors have declared that no competing interests exist.

Transparency document

The Transparency document associated with this article can be found, in the online version.

Acknowledgments

We thank T. Penkauskas for the assistance in preparing tBLMs and setting up EIS experiments, H. Jost and S. Billington (University of Arizona, USA) for the rPLO plasmid and M. Palmer (University of Waterloo, Canada) for the dsPLO plasmid, and D.J. Vanderah and Z. Sallman for purification of the molecular anchor HC18 for tBLMs used for neutron reflectometry. The authors gratefully acknowledge the European Social Fund for the financial support through the agreement no. VP1-3.1-ŠMM-10-V-02-024 (project MiniFob). G.V. acknowledges the University of Maryland Institute for Biosciences and Biotechnology Research (Rockville, Maryland) for the travel support and NIST Center for Neutron Research for access to neutron instrumentation.

References

[1] C.J. Rosado, S. Kondos, T.E. Bull, M.J. Kuiper, R.H. Law, A.M. Buckle, I. Voskoboinik, P.I. Bird, J.A. Trapani, J.C. Whisstock, M.A. Dunstone, The MACPF/CDC family of pore-forming toxins, Cell. Microbiol. 10 (2008) 1765–1774.
[2] E.M. Hotze, R.K. Tweten, Membrane assembly of the cholesterol-dependent cytolysin pore complex, Biochim. Biophys. Acta 1818 (2012) 1028–1038.
[3] M.A. Dunstone, R.K. Tweten, Packing a punch: the mechanism of pore formation by cholesterol dependent cytolysins and membrane attack complex/perforin-like proteins, Curr. Opin. Struct. Biol. 22 (2012) 342–349.
[4] R. Ramachandran, R.K. Tweten, A.E. Johnson, Membrane-dependent conformational changes initiate cholesterol-dependent cytolysin oligomerization and intersubunit beta-strand alignment, Nat. Struct. Mol. Biol. 11 (2004) 697–705.
[5] B.H. Jost, S.J. Billington, Arcanobacterium pyogenes: molecular pathogenesis of an animal opportunist, Antonie Van Leeuwenhoek 88 (2005) 87–102.
[6] R.J. Goldstone, M. Amos, R. Talbot, H.J. Schuberth, O. Sandra, I.M. Sheldon, D.G. Smith, Draft genome sequence of *Trueperella pyogenes*, isolated from the infected uterus of a postpartum cow with Metritis, Genome Announc. 2 (2014).
[7] G. Preta, V. Lotti, J.G. Cronin, I.M. Sheldon, Protective role of the dynamin inhibitor Dynasore against the cholesterol-dependent cytolysin of *Trueperella pyogenes*, FASEB J. 29 (2015) 1516–1528.
[8] A. Zvirbliene, M. Pleckaityte, R. Lasickiene, I. Kucinskaite-Kodze, G. Zvirblis, Production and characterization of monoclonal antibodies against vaginolysin: mapping of a region critical for its cytolytic activity, Toxicon 56 (2010) 19–28.
[9] R. Budvytyte, M. Pleckaityte, A. Zvirbliene, D.J. Vanderah, G. Valincius, Reconstitution of cholesterol-dependent vaginolysin into tethered phospholipid bilayers: implications for bioanalysis, PLoS One 8 (2013), e82536.
[10] G. Valincius, T. Meskauskas, F. Ivanauskas, Electrochemical impedance spectroscopy of tethered bilayer membranes, Langmuir 28 (2012) 977–990.
[11] G. Valincius, D.J. McGillivray, W. Febo-Ayala, D.J. Vanderah, J.J. Kasianowicz, M. Losche, Enzyme activity to augment the characterization of tethered bilayer membranes, J. Phys. Chem. B 110 (2006) 10213–10216.
[12] B.A. Cornell, V.L. Braach-Maksvytis, L.G. King, P.D. Osman, B. Raguse, L. Wieczorek, R.J. Pace, A biosensor that uses ion-channel switches, Nature 387 (1997) 580–583.
[13] M. Andersson, H.M. Keizer, C. Zhu, D. Fine, A. Dodabalapur, R.S. Duran, Detection of single ion channel activity on a chip using tethered bilayer membranes, Langmuir 23 (2007) 2924–2927.
[14] B. Rakovska, T. Ragaliauskas, M. Mickevicius, M. Jankunec, G. Niaura, D.J. Vanderah, G. Valincius, Structure and function of the membrane anchoring self-assembled monolayers, Langmuir 31 (2015) 846–857.
[15] I. Horcas, R. Fernandez, J.M. Gomez-Rodriguez, J. Colchero, J. Gomez-Herrero, A.M. Baro, WSXM: a software for scanning probe microscopy and a tool for nanotechnology, Rev. Sci. Instrum. 78 (2007) 013705.
[16] A. Mikhailov, S.K. Sekatskii, G. Dietler, DNA trace: a comprehensive software for polymer image processing, J. Adv. Microsc. Res. 8 (2013) 241–245 (245).
[17] J.A. Dura, D.J. Pierce, C.F. Majkrzak, N.C. Maliszewskyj, D.J. McGillivray, M. Losche, K.V. O'Donovan, M. Mihailescu, U. Perez-Salas, D.L. Worcester, S.H. White, AND/R: advanced neutron diffractometer/reflectometer for investigation of thin films and multilayers for the life sciences, Rev. Sci. Instrum. 77 (2006) 74301–74311.
[18] B.J. Kirby, P.A. Kienzle, B.B. Maranville, N.F. Berk, J. Krycka, F. Heinrich, C.F. Majkrzak, Phase-sensitive specular neutron reflectometry for imaging the nanometer scale composition depth profile of thin-film materials, Curr. Opin. Colloid Interface Sci. 17 (2012) 44–53.
[19] J.F. Ankner, C.F. Majkrzak, Subsurface profile refinement for neutron specular reflectivity, Neutron Opt. Devices Appl. 1738 (1992) 260–269.
[20] P. Shekhar, H. Nanda, M. Losche, F. Heinrich, Continuous distribution model for the investigation of complex molecular architectures near interfaces with scattering techniques, J. Appl. Phys. 110 (2011) (102216-102216-102212).
[21] F. Heinrich, M. Losche, Zooming in on disordered systems: neutron reflection studies of proteins associated with fluid membranes, Biochim. Biophys. Acta 1838 (2014) 2341–2349.
[22] S.J. Billington, B.H. Jost, W.A. Cuevas, K.R. Bright, J.G. Songer, The *Arcanobacterium* (Actinomyces) *pyogenes* hemolysin, pyolysin, is a novel member of the thiol-activated cytolysin family, J. Bacteriol. 179 (1997) 6100–6106.
[23] M. Zilnyte, C. Venclovas, A. Zvirbliene, M. Pleckaityte, The cytolytic activity of vaginolysin strictly depends on cholesterol and is potentiated by human CD59, Toxins 7 (2015) 110–128.
[24] M.R. Amos, G.D. Healey, R.J. Goldstone, S.M. Mahan, A. Duvel, H.J. Schuberth, O. Sandra, P. Zieger, I. Dieuzy-Labaye, D.G. Smith, I.M. Sheldon, Differential endometrial cell sensitivity to a cholesterol-dependent cytolysin links *Trueperella pyogenes* to uterine disease in cattle, Biol. Reprod. 90 (2014) 54.
[25] O. Eicher-Lorka, T. Charkova, A. Matijoska, Z. Kuodis, G. Urbelis, T. Penkauskas, M. Mickevicius, A. Bulovas, G. Valincius, Cholesterol-based tethers and markers for model membranes investigation, Chem. Phys. Lipids 195 (2016) 71–86.

[26] G. Valincius, M. Mickevicius, Tethered phospholipid bilayer membranes: an interpretation of the electrochemical impedance response, Adv. Planar Lipid Bilayers Liposomes 21 (2015) 27–61.
[27] B.A. Cornell, G. Krishna, P.D. Osman, R.D. Pace, L. Wieczorek, Tethered-bilayer lipid membranes as a support for membrane-active peptides, Biochem. Soc. Trans. 29 (2001) 613–617.
[28] J. Kozuch, C. Steinem, P. Hildebrandt, D. Millo, Combined electrochemistry and surface-enhanced infrared absorption spectroscopy of gramicidin A incorporated into tethered bilayer lipid membranes, Angew. Chem. 51 (2012) 8114–8117.
[29] D.J. McGillivray, G. Valincius, F. Heinrich, J.W. Robertson, D.J. Vanderah, W. Febo-Ayala, I. Ignatjev, M. Losche, J.J. Kasianowicz, Structure of functional *Staphylococcus aureus* alpha-hemolysin channels in tethered bilayer lipid membranes, Biophys. J. 96 (2009) 1547–1553.
[30] S.M. Valenzuela, H. Alkhamici, L.J. Brown, O.C. Almond, S.C. Goodchild, S. Carne, P.M.G. Curmi, S.A. Holt, B.A. Cornell, Regulation of the membrane insertion and conductance activity of the metamorphic Chloride Intracellular Channel protein CLIC1 by cholesterol, PLoS One 8 (2013).
[31] L. Pokrajac, C. Baik, J.R. Harris, N.S. Sarraf, M. Palmer, Partial oligomerization of pyolysin induced by a disulfide-tethered mutant, Biochem. Cell Biol. (Biochimie et biologie cellulaire), 90 (2012) 709–717.
[32] A.D. Donkor, Z.D. Su, H.S. Mandal, X. Jin, X.W. Tang, Carbon nanotubes inhibit the hemolytic activity of the pore-forming toxin pyolysin, Nano Res. 2 (2009) 517–525.
[33] C. Leung, N.V. Dudkina, N. Lukoyanova, A.W. Hodel, I. Farabella, A.P. Pandurangan, N. Jahan, M.P. Damaso, D. Osmanovic, C.F. Reboul, M.A. Dunstone, P.W. Andrew, R. Lonnen, M. Topf, H.R. Saibil, B.W. Hoogenboom, Stepwise visualization of membrane pore formation by suilysin, a bacterial cholesterol-dependent cytolysin, Elife 3 (2014).
[34] R. Blumenthal, S.A. Gallo, M. Viard, Y. Raviv, A. Puri, Fluorescent lipid probes in the study of viral membrane fusion, Chem. Phys. Lipids 116 (2002) 39–55.
[35] O. Maier, V. Oberle, D. Hoekstra, Fluorescent lipid probes: some properties and applications (a review), Chem. Phys. Lipids 116 (2002) 3–18.
[36] E. Girard, J.L. Paul, N. Fournier, P. Beaune, L. Johannes, C. Lamaze, B. Vedie, The dynamin chemical inhibitor dynasore impairs cholesterol trafficking and sterol-sensitive genes transcription in human HeLa cells and macrophages, PLoS One 6 (2011), e29042.
[37] G. Preta, J.G. Cronin, I.M. Sheldon, Dynasore — not just a dynamin inhibitor, Cell Commun. Signal. 13 (2015) 24.
[38] A. Junghans, C. Champagne, P. Cayot, C. Loupiac, I. Koper, Probing protein–membrane interactions using solid supported membranes, Langmuir 27 (2011) 2709–2716.
[39] G. Valincius, F. Heinrich, R. Budvytyte, D.J. Vanderah, D.J. McGillivray, Y. Sokolov, J.E. Hall, M. Losche, Soluble amyloid beta-oligomers affect dielectric membrane properties by bilayer insertion and domain formation: implications for cell toxicity, Biophys. J. 95 (2008) 4845–4861.
[40] S.J. Tilley, E.V. Orlova, R.J. Gilbert, P.W. Andrew, H.R. Saibil, Structural basis of pore formation by the bacterial toxin pneumolysin, Cell 121 (2005) 247–256.
[41] J.J. Kasianowicz, S.M. Bezrukov, Protonation dynamics of the alpha-toxin ion channel from spectral analysis of pH-dependent current fluctuations, Biophys. J. 69 (1995) 94–105.
[42] D.W. Schuerch, E.M. Wilson-Kubalek, R.K. Tweten, Molecular basis of listeriolysin O pH dependence, Proc. Natl. Acad. Sci. U. S. A. 102 (2005) 12537–12542.
[43] R. Rampersaud, P.J. Planet, T.M. Randis, R. Kulkarni, J.L. Aguilar, R.I. Lehrer, A.J. Ratner, Inerolysin, a cholesterol-dependent cytolysin produced by *Lactobacillus iners*, J. Bacteriol. 193 (2011) 1034–1041.
[44] M.S. Khan, N.S. Dosoky, J.D. Williams, Engineering lipid bilayer membranes for protein studies, Int. J. Mol. Sci. 14 (2013) 21561–21597.
[45] J.D. Taylor, M.J. Linman, T. Wilkop, Q. Cheng, Regenerable tethered bilayer lipid membrane arrays for multiplexed label-free analysis of lipid–protein interactions on poly(dimethylsiloxane) microchips using SPR imaging, Anal. Chem. 81 (2009) 1146–1153.
[46] E. Macia, M. Ehrlich, R. Massol, E. Boucrot, C. Brunner, T. Kirchhausen, Dynasore, a cell-permeable inhibitor of dynamin, Dev. Cell 10 (2006) 839–850.
[47] T. Kirchhausen, E. Macia, H.E. Pelish, Use of dynasore, the small molecule inhibitor of dynamin, in the regulation of endocytosis, Methods Enzymol. 438 (2008) 77–93.
[48] R.J. Park, H. Shen, L. Liu, X. Liu, S.M. Ferguson, P. De Camilli, Dynamin triple knockout cells reveal off target effects of commonly used dynamin inhibitors, J. Cell Sci. 126 (2013) 5305–5312.
[49] X. Zhang, W. Fu, C.G. Palivan, W. Meier, Natural channel protein inserts and functions in a completely artificial, solid-supported bilayer membrane, Sci. Rep. 3 (2013) 2196.
[50] L. Ginsberg, Does Ca^{2+} cause fusion or lysis of unilamellar lipid vesicles? Nature 275 (1978) 758–760.
[51] I.K. Vockenroth, P.P. Atanasova, A.T. Jenkins, I. Koper, Incorporation of alpha-hemolysin in different tethered bilayer lipid membrane architectures, Langmuir 24 (2008) 496–502.
[52] Y. Liu, Z. Zhang, Q. Zhang, G.L. Baker, R.M. Worden, Biomembrane disruption by silica-core nanoparticles: effect of surface functional group measured using a tethered bilayer lipid membrane, Biochim. Biophys. Acta 1838 (2014) 429–437.